Simple transfer functions for calculating benthic fixed nitrogen losses and C:N:P regeneration ratios in global biogeochemical models

Lisa Bohlen,[1] Andrew W. Dale,[1] and Klaus Wallmann[1]

Received 5 September 2011; revised 8 May 2012; accepted 12 August 2012; published 25 September 2012.

[1] Empirical transfer functions are derived for predicting the total benthic nitrate loss (L_{NO3}) and the net loss of dissolved inorganic nitrogen (L_{DIN}) in marine sediments, equivalent to sedimentary denitrification. The functions are dynamic vertically integrated sediment models which require the rain rate of particulate organic carbon to the seafloor (RRPOC) and a proposed new variable $(O_2\text{-}NO_3)_{bw}$ (bottom water O_2 concentration minus NO_3^- concentration) as the only input parameters. Applied globally to maps of RRPOC and $(O_2\text{-}NO_3)_{bw}$ on a $1^\circ \times 1^\circ$ spatial resolution, the models predict a NO_3^- drawdown of 196 Tg yr^{-1} (L_{NO3}) of which 153 – 155 Tg yr^{-1} is denitrified to N_2 (L_{DIN}). This is in good agreement with previous estimates using very different methods. Our approach implicitly accounts for fixed N loss via anammox, such that our findings do not support the idea that the relatively recent discovery of anammox in marine sediments might require current estimates of the global benthic marine N budget to be revised. The continental shelf (0 – 200 m) accounts for >50% of global L_{NO3} and L_{DIN}, with slope (200 – 2000 m) and deep-sea (>2000 m) sediments contributing ca. 30% and 20%, respectively. Denitrification in high-nitrate/low-oxygen regions such as oxygen minimum zones is significant (ca. 15 Tg N yr^{-1}; 10% of global) despite covering only ~1% of the seafloor. The data are used to estimate the net fluxes of nitrate (18 Tg N yr^{-1}) and phosphate (27 Tg P yr^{-1}) across the sediment-water interface. The benthic fluxes strongly deviate from Redfield composition, with globally averaged N:P, N:C and C:P values of 8.3, 0.067 and 122, respectively, indicating world-wide fixed N losses (by denitrification) relative to C and P. The transfer functions are designed to be coupled dynamically to general circulation models to better predict the feedback of sediments on pelagic nutrient cycling and dissolved O_2 distributions.

Citation: Bohlen, L., A. W. Dale, and K. Wallmann (2012), Simple transfer functions for calculating benthic fixed nitrogen losses and C:N:P regeneration ratios in global biogeochemical models, *Global Biogeochem. Cycles*, *26*, GB3029, doi:10.1029/2011GB004198.

1. Introduction

[2] The marine fixed nitrogen (N) budget of the global ocean is poorly constrained due to uncertainty in the magnitude of the major input fluxes by nitrogen fixation and removal fluxes by denitrification. Benthic denitrification is believed to be the major sink for fixed nitrogen [*Codispoti et al.*, 2001; *Brandes and Devol*, 2002; *Galloway et al.*, 2004; *Gruber*, 2004]. Early estimates of global benthic denitrification rates pointed toward values on the order of 100 Tg N y^{-1} or lower [e.g., *Codispoti and Christensen*, 1985]. More recently, however, these estimates have been revised upwards by as much as a factor of 2 – 3 using a variety of different approaches such as global N isotope budgeting [*Brandes and Devol*, 2002; *Deutsch et al.*, 2004], reaction–transport modeling [*Middelburg et al.*, 1996] and data extrapolation and interpretation [*Codispoti et al.*, 2001]. Nonetheless, benthic denitrification, and preferential nutrient retention and release in general, are only rarely considered in global biogeochemical models of N cycling [e.g., *Romaniello and Derry*, 2010; *Somes et al.*, 2010].

[3] Shelf and hemipelagic sediments have been identified as important sites for denitrification [*Christensen et al.*, 1987; *Devol*, 1991]. In recent decades, progress has been made in determining the factors that ultimately control the rate of benthic denitrification that explain these observations. Using a diagenetic model forced by parameterizations based on seafloor bathymetry, *Middelburg et al.* [1996] observed that denitrification in deep-sea sediments was

[1]Helmholtz Centre for Ocean Research Kiel, Kiel, Germany.

Corresponding author: L. Bohlen, Helmholtz Centre for Ocean Research Kiel, Wischhofstrasse 1-3, DE-24148 Kiel, Germany. (lbohlen@geomar.de)

0886-6236/12/2011GB004198

most sensitive to the rain rate of labile particulate organic carbon (POC) to the seafloor. However, nitrate (NO_3^-) concentrations are also important, particularly for high nitrate low oxygen (HNLO) waters that are depleted in dissolved oxygen (O_2) [e.g., *Fennel et al.*, 2009; *Dale et al.*, 2011]. Even though most denitrifying bacteria are facultative anaerobes [*Tiedje*, 1988], the effect of bottom water O_2 is less obvious. For example, higher O_2 concentrations may either lead to an enhancement of denitrification via coupled nitrification-denitrification or may inhibit denitrification though reduced substrate availability because of higher aerobic respiration rates [*Rysgaard et al.*, 1994; *Middelburg et al.*, 1996]. Ultimately, the relative concentrations of O_2 and NO_3^- appear to be critical in determining benthic denitrification rates if organic substrate is plentiful [*Dale et al.*, 2011].

[4] The aim of this study is to derive predictive algorithms, or transfer functions, for depth-integrated denitrification rates and nutrient regeneration ratios in marine sediments based on a small number of globally accessible parameters. The transfer functions are equivalent to the 'level 3' dynamic vertically-integrated sediment model described by *Soetaert et al.* [2000] for coupling benthic and pelagic biogeochemical models. To achieve this, we first developed a function for total benthic NO_3^- losses (L_{NO3}) using measured NO_3^- fluxes across the sediment-water interface. L_{NO3} is equivalent to the maximum rate of denitrification because it does not account for the release of fixed N as ammonium (NH_4^+) back to the water column. Thus, in a second step, L_{NO3} was corrected using observed NH_4^+ fluxes, giving the net loss of dissolved inorganic nitrogen, L_{DIN} (DIN = NO_3^- + NH_4^+). L_{DIN} is then used as a proxy for benthic denitrification. Based on previous results [*Middelburg et al.*, 1996; *Dale et al.*, 2011], bottom water O_2 and NO_3^- concentrations and the rain rate of POC to the seafloor (RRPOC) were used as master variables in the transfer function through a proposed new variable $(O_2\text{-}NO_3)_{bw}$ (= bottom water O_2 concentrations minus NO_3^-). These functions are then applied to global fields of $(O_2\text{-}NO_3)_{bw}$ and RRPOC to derive new estimates of benthic denitrification that are consistent with previous estimates. Finally, we used a model for carbon-to-phosphorus regeneration ratios in marine sediments developed by *Wallmann* [2010] to derive global maps of the ratios of C, N and P fluxes in shelf, slope, deep-sea and HNLO regions. These easy-to-apply functions are designed to be coupled to biogeochemical general circulation models as a computationally efficient means of evaluating potential benthic feedbacks on the global inventory of ocean fixed N, P and dissolved O_2.

2. Data Acquisition

2.1. Site Specific Data

[5] Literature data of NO_3^- (J_{NO3}) and NH_4^+ (J_{NH4}) fluxes across the sediment-water interface, bottom water O_2 (μM) and NO_3^- (μM) concentrations and total benthic carbon oxidation rates (C_{ox}, mmol C m^{-2} d^{-1}) from sites all over the world were compiled. A global map and table listing all sites is provided in the auxiliary material (Figure S1 and Table S1).[1] At stations where bottom water O_2 and NO_3^- concentrations were not provided in the original references, these values were estimated from nearby stations or from the World Ocean Atlas (WOA) 2005 [*Garcia et al.*, 2006a, 2006b]. Since the rate of solute transport across the sediment-water interface by bioirrigation may be up to 3 times higher than the molecular diffusive flux [*Devol and Christensen*, 1993], only in situ fluxes using benthic chamber deployments were included in the database. However, for water depths >3000 m, bioirrigation was assumed to be of minor importance [*Glud*, 2008] and diffusive fluxes determined ex situ from pore water profiles were used in addition to in situ chamber measurements. A total of 180 NO_3^- and 122 NH_4^+ flux measurements were available. In this work, negative fluxes denote uptake by the sediment.

[6] The transfer functions require knowledge of RRPOC as an input parameter. However, in almost all cases only C_{ox} was given (see Table S1 in the auxiliary material). RRPOC was therefore calculated by assuming that the accumulation rate of POC below the bioturbated zone (APOC, mmol C m^{-2} d^{-1}) is equal to the difference between RRPOC and C_{ox} at steady state:

$$\mathrm{APOC} = \mathrm{RRPOC} - C_{ox} \tag{1}$$

This equation introduces an unknown, APOC. To eliminate APOC, we used the following equations that relate RRPOC and APOC in shelf/slope (<2000 m) and deep-sea (>2000 m) sediments [*Flögel et al.*, 2011]:

$$\mathrm{APOC} = \begin{cases} 0.14 \times \mathrm{RRPOC}^{1.11} & \text{for water depths} \le 2000\,\mathrm{m} \\ 0.014 \times \mathrm{RRPOC}^{1.05} & \text{for water depths} \ge 2000\,\mathrm{m} \end{cases} \tag{2}$$

RRPOC values were then obtained by solving equations (1) and (2). Note that equation (2) is a nonlinear function in RRPOC, such that the burial correction of the rain rate may be >20% in cases with high rain rates in shelf settings, leading to a significant effect on derived global denitrification rates. The burial correction for the deep sea has a negligible impact on the global denitrification rate and is included for completion only.

2.2. Completeness of the Database

[7] The database covers the broad range of redox conditions encountered in the contemporary ocean, including sites from intense HNLO regions (i.e., anoxic oxygen minimum zones) to fully oxygenated regions of the ocean from the shallow shelf to the deep sea (see auxiliary material). Observed J_{NO3} (mmol N m^{-2} d^{-1}) were directed both into and out of the sediment, yet higher rates were found for NO_3^- uptake (Figure 1a). Maximum NO_3^- uptake rates occurred on the shelf and slope in conjunction with high J_{NH4} (Figure 1b) and RRPOC (Figure 1c). These are also sites with low bottom water O_2 concentrations, and maximum uptake rates in our database corresponded to the highly productive oxygen minimum zone (OMZ) off Peru [*Bohlen et al.*, 2011], northwest Mexico and Washington [*Devol and Christensen*, 1993; *Hartnett and Devol*, 2003]. Release of NO_3^- was often observed at sites with low bottom water NO_3^- concentrations that drive an upward diffusive flux of NO_3^- and at sites with well-oxygenated bottom waters and low benthic carbon degradation rates that favor nitrification of NH_4^+ to NO_3^- [e.g., *Hammond et al.*, 1999]. The range of J_{NO3} and J_{NH4}

[1] Auxiliary materials are available in the HTML. doi:10.1029/2011GB004198.

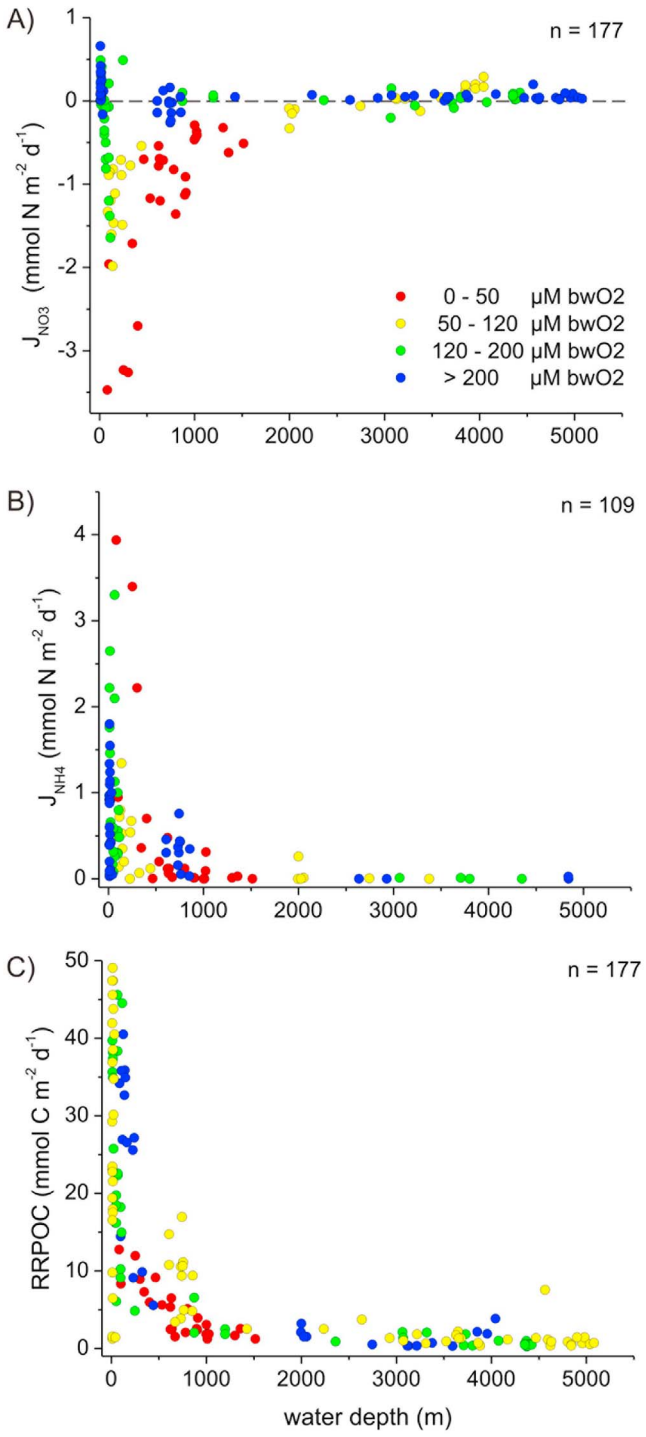

Figure 1. Benthic fluxes (mmol m^{-2} d^{-1}) as a function of water depth (m). (a) NO_3^- (including NO_2^- data where provided); (b) NH_4^+; (c) organic carbon rain rates (RRPOC). Negative fluxes denote uptake by the sediment.

in the data set is similar to that reported by *Middelburg et al.* [1996] in their global denitrification study.

[8] Maximum J_{NH4} values occurred at shallow water depths (Figure 1b). Very high fluxes (≥2 mmol NH_4^+ m^{-2} d^{-1}) were found for sites exhibiting normal oxic bottom water conditions and high POC degradation rates of ≥17 mmol C m^{-2} d^{-1} [e.g., *Hammond et al.*, 1999], probably as a result of high ammonification and concomitant NH_4^+ release by bioirrigation [*Dale et al.*, 2011]. However, fluxes in the same range were also reported for the Peruvian OMZ [*Bohlen et al.*, 2011] despite lower POC degradation rates (~6 – 8 mmol C m^{-2} d^{-1}). These high NH_4^+ fluxes result from the activity of giant sulfur bacteria performing DNRA [*Bohlen et al.*, 2011]. In HNLO environments, DNRA can be an important source of NH_4^+ [e.g., *Otte et al.*, 1999], but may also be significant in more oxygenated settings, especially those where hypoxia occurs on variable time scales [*Dale et al.*, 2011].

[9] Carbon rain rates ranged from 0.3 – 50 mmol C m^{-2} d^{-1} with highest values on the shelf as expected, and decreased down the continental slope (Figure 1c). The wide range of values on the shelf may be related to regional differences in primary production or particle settling velocities [*Rullkötter*, 2006]. This variability in rain rate ensures that a wide range of carbon deposition environments is included in the derivation of the transfer functions below.

3. Derivation of the Transfer Function

3.1. Defining Benthic NO_3^- and DIN Loss

[10] J_{NO3} and C_{ox} were used to calculate the depth–integrated rate of NO_3^- loss (L_{NO3}):

$$L_{NO3} = RPON - J_{NO3} = C_{ox} \times 16/106 - J_{NO3} \quad (3)$$

where RPON is the degradation of particulate organic nitrogen determined from C_{ox} with a Redfield C:N ratio of 106:16. Thus, NO_3^- losses are highest when J_{NO3} is negative (benthic uptake), and vice versa. The concept behind the foregoing equation relies on the idea that all particulate organic nitrogen mineralized as NH_4^+ is directly coupled to nitrification at steady state (Figure 2). We consider that nitrite does not accumulate to significant levels in the sediment or water column to warrant inclusion of this reactive intermediate in the conceptual model. Thus, in view of this highly simplified reaction network, our model does not differentiate between fixed N loss to N_2 by canonical denitrification or anammox, but instead provides the sum of these potential pathways. Furthermore, solute burial is considered to be negligible compared to diffusion and is ignored in these calculations. In what follows, the term denitrification refers to combined canonical denitrification and anammox.

[11] Highly irrigated organic-rich shelf sediments and those underlying hypoxic bottom waters may release NH_4^+ directly to the overlying water column. Since equation (3) ignores the potential efflux of NH_4^+, fixed N losses estimated using this equation represents the maximum potential denitrification rate. L_{NO3} can be corrected to give an expression for the net loss of DIN (L_{DIN}) which is a more realistic estimate of denitrification:

$$L_{DIN} = L_{NO3} - J_{NH4} = C_{ox} \times 16/106 - J_{NO3} - J_{NH4} \quad (4)$$

Note that dissimilatory nitrate reduction to ammonium (DNRA) by giant sulfur bacteria such as *Beggiatoa* [e.g., *Otte et al.*, 1999] was not considered explicitly as a sink for NO_3^- (Figure 2). However, this process is implicitly accounted for in the L_{DIN} estimate since the NH_4^+ produced

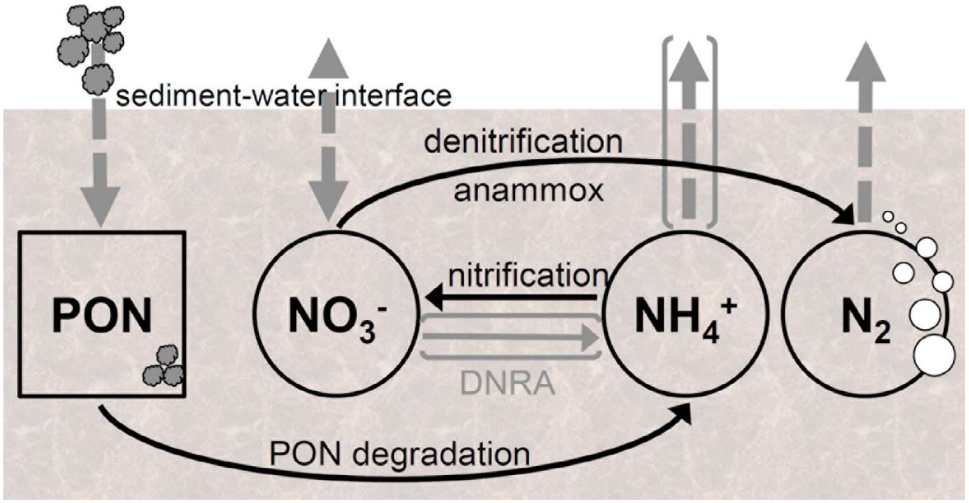

Figure 2. Conceptual model of the reaction network used to derive the transfer function. The arrow in brackets symbolizes the potential fluxes of NH_4^+ across the sediment-water interface which was considered for the calculation of net DIN loss (see section 3.1). Note that NO_3^- is defined as the sum of $NO_3^- + NO_2^-$.

by DNRA will be either nitrified to NO_3^- or released from the sediment as NH_4^+. Only sites with positive L_{NO3} and L_{DIN} values determined from equations (3) and (4) were considered for further analysis. Negative values imply that more NO_3^- and/or NH_4^+ are released than produced in situ. N cycling at such sites (e.g., some stations on the Porcupine Abyssal Plain or in the Equatorial Pacific) may not be at steady state or, alternatively, organic matter mineralization may be occurring with C:N ratios lower than Redfield. While there is some evidence to suggest a non-Redfield composition of organic material in marine sediments [e.g., *Müller*, 1977], a constant C:N is considered here so as to be consistent with the commonly assumed Redfield stoichiometry adopted in general circulation biogeochemical models.

3.2. A Transfer Function for Denitrification

[12] A transfer function for predicting total benthic NO_3^- loss was derived using RRPOC and bottom water O_2 (μM) and NO_3^- (μM) concentrations as master variables. Previous studies have shown that denitrification and anammox are highly sensitive to these variables [*Middelburg et al.*, 1996; *Dalsgaard et al.*, 2005; *Dale et al.*, 2011]. Since denitrification rates are elevated in HNLO regions [e.g., *Devol and Christensen*, 1993], a new variable $(O_2\text{-}NO_3)_{bw}$ (= bottom water O_2 concentration minus NO_3^- concentration) is proposed to embrace this observation. $(O_2\text{-}NO_3)_{bw}$ describes HNLO settings as negative values and normal oxic waters as highly positive values. Using the information in our database we identified a relationship between L_{NO3} (mmol N m^{-2} d^{-1}), RRPOC (mmol C m^{-2} d^{-1}) and $(O_2\text{-}NO_3)_{bw}$ (μM):

$$\frac{L_{NO3}}{RRPOC} = a + b \times c^{(O_2 - NO_3)_{bw}} \quad (5)$$

where $a = 0.083 \pm 0.006$, $b = 0.21 \pm 0.013$ and $c = 0.98 \pm 0.002$. This function shown in Figure 3a ($r^2 = 0.78$, n = 180, $p < 0.001$) indicates that the rate of N loss per mol of carbon deposited on the seafloor (= L_{NO3}/RRPOC) increases as $(O_2\text{-}NO_3)_{bw}$ decreases. Rearranging equation (5) gives the transfer function for NO_3^- loss:

$$L_{NO3} = \left(a + b \times c^{(O_2 - NO_3)_{bw}}\right) \times RRPOC \quad (6)$$

The error or uncertainty in equation (5), $\Delta(L_{NO3}/RRPOC)$, was determined from the residuals of the fit against the data. As shown in Figure 3b, $\Delta(L_{NO3}/RRPOC)$ is not constant but increases with decreasing $(O_2\text{-}NO_3)_{bw}$ (Figure 3b) according to the function:

$$\Delta\frac{L_{NO3}}{RRPOC} = d + e \times f^{(O_2 - NO_3)_{bw}} \quad (7)$$

where $d = -0.0047 \pm 0.015$, $e = 0.085 \pm 0.016$ and $f = 0.99 \pm 0.002$. Using error combination rules, ΔL_{NO3} was calculated from $\Delta(L_{NO3}/RRPOC)$ and the mean relative error of the POC rain rate (ΔRRPOC/RRPOC):

$$\Delta L_{NO3} = L_{NO3}\sqrt{\left(\frac{\Delta\left(\frac{L_{NO3}}{RRPOC}\right)}{\frac{L_{NO3}}{RRPOC}}\right)^2 - \left(\frac{\Delta RRPOC}{RRPOC}\right)^2} \quad (8)$$

The relative error in the rain rate was estimated as 20% based on confidence limits of benthic total oxygen uptake in a global study by *Andersson et al.* [2004].

[13] By ignoring the NH_4^+ efflux, L_{NO3}/RRPOC represents the maximum fraction of RRPOC that is denitrified. Therefore, two different approaches, *a priori* and *a posteriori*, were used to correct L_{NO3} for the NH_4^+ flux. In the *a priori* approach, we identified (Figure 3c) a correlation between L_{DIN}, RRPOC and $(O_2\text{-}NO_3)_{bw}$ in the same way as for L_{NO3} ($r^2 = 0.67$, $p < 0.001$, n = 122):

$$\frac{L_{DIN}}{RRPOC} = a + b \times c^{(O_2 - NO_3)_{bw}} \quad (9)$$

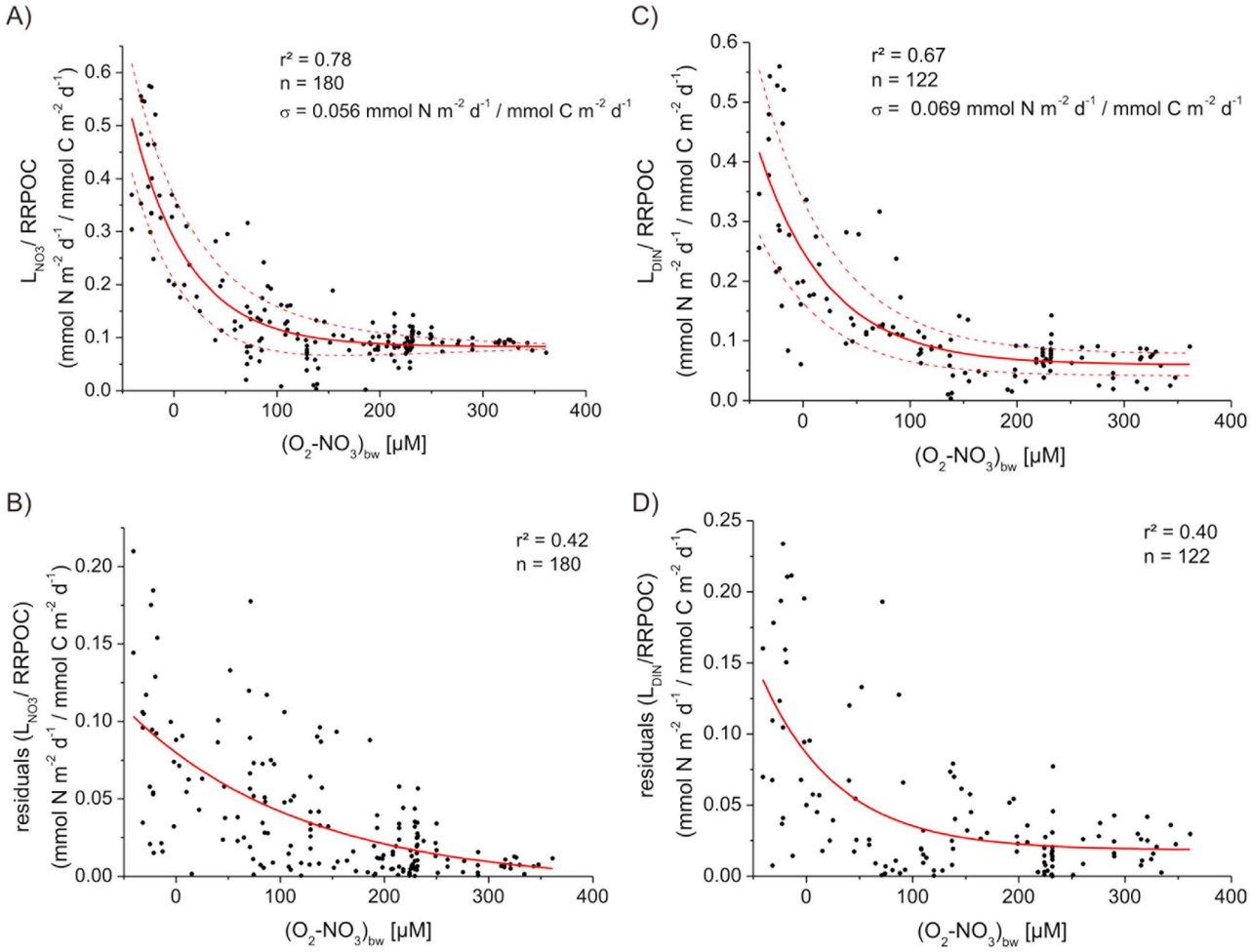

Figure 3. The ratio of (a) L_{NO3}/RRPOC and (c) L_{DIN}/RRPOC as a function of $(O_2\text{-}NO_3)_{bw}$. The solid lines show the nonlinear fit through the data (equations (5) and (9)) and the dotted lines denote the error estimated from the residuals given in Figures 3b and 3d. The nonlinear fit through the residuals (equations (7) and (11)) is denoted by the solid line with the standard deviation (σ) and the correlation coefficient (r^2) indicated.

where here $a = 0.060 \pm 0.01$, $b = 0.19 \pm 0.019$, $c = 0.99 \pm 0.003$. Rearranging equation (9) gives an estimate for benthic denitrification which we will denote DEN1:

$$\mathrm{DEN1} = L_{DIN} = \left(a + b \times c^{(O_2 - NO_3)_{bw}}\right) \times \mathrm{RRPOC} \qquad (10)$$

with the uncertainty given as:

$$\Delta \frac{L_{DIN}}{\mathrm{RRPOC}} = d + e \times f^{(O_2 - NO_3)_{bw}} \qquad (11)$$

where $d = 0.018 \pm 0.007$, $e = 0.068 \pm 0.011$ and $f = 0.99 \pm 0.004$ (Figure 3d). The error for the *a priori* denitrification estimate, ΔDEN1, was calculated analogous to equation (8).

[14] In the second approach, the correction for benthic NH_4^+ efflux to L_{NO3} was done *a posteriori* using as a fixed percentage of the measured NH_4^+ flux to total NO_3^- loss (Figure S2 in the auxiliary material). NH_4^+ release was generally minor for water depths >1000 m and for these sites we assumed that the calculated L_{NO3} equals the total loss of fixed N in the sediment. In contrast, NH_4^+ effluxes were equivalent to as much as 80% of NO_3^- fluxes for water depths <1000 m. The NH_4^+ flux showed no robust correlation with RRPOC and $(O_2\text{-}NO_3)_{bw}$ (data not shown). Therefore, as a first approximation, we assumed that for water depths <1000 m the NH_4^+ flux was equal to the average fraction of the NO_3^- flux for these water depths, that is, 27 ± 23% of L_{NO3}. The a posteriori benthic denitrification estimate (DEN2) is thus calculated by correcting the transfer function for the NO_3^- loss (equation (6)) directly:

$$\mathrm{DEN2} = \begin{cases} L_{NO3} & \text{for water depths} \geq 1000\,\mathrm{m} \\ 0.73 \times L_{NO3} & \text{for water depths} \leq 1000\,\mathrm{m} \end{cases} \qquad (12)$$

3.3. Stoichiometry of Benthic N and P Fluxes

[15] The transfer functions for benthic NO_3^- and DIN losses allow the flux of NO_3^- (J_{NO3}) and DIN (J_{DIN}) across the sediment-water interface to be estimated:

$$J_{NO3} = C_{ox} \times 16/106 - L_{NO3} \qquad (13)$$

$$J_{DIN} = C_{ox} \times 16/106 - L_{DIN} \qquad (14)$$

Where C_{ox} was estimated from globally-extrapolated rain rate values (see Section 4.1). Note that J_{NO3} includes NO_3^- uptake by denitrification and DNRA, whereas J_{DIN} corrects for any potential NO_3^- consumption by DNRA. The derived and measured J_{NO3} are significantly correlated ($r^2 = 0.87$, n = 180, p <0.001) (Figure S3 in the auxiliary material). The measured DIN fluxes were also reproduced significantly by equation (14) ($r^2 = 0.70$, n = 122, p <0.001). *Wallmann* [2010] collated literature data of worldwide benthic phosphate effluxes (J_{PO4}) (mmol P m^{-2} d^{-1}), bottom water O_2 concentrations (μM) and, together with C_{ox} (mmol C m^{-2} d^{-1}), derived a relationship for the C:P regeneration ratio in marine sediments, that is, the number of moles of POC mineralized per mole of PO_4^{3-} released (r_{REG}):

$$r_{REG} = \frac{C_{ox}}{J_{PO4}} = a - b \times \exp\left(\frac{-O_2}{c}\right) \quad (15)$$

where *a* (123), *b* (112) and *c* (32 μM) are empirical constants [*Wallmann*, 2010]. This function shows that r_{REG} is higher than Redfield under oxic conditions, indicating preferential P burial in most sedimentary environments. However, excess P is strongly released from continental margins when O_2 <20 μM [*Wallmann*, 2010]. Rearrangement of equation (15) enables the calculation of J_{PO4} directly:

$$J_{PO4} = \frac{C_{ox}}{a - b \times \exp\left(\frac{-O_2}{c}\right)} \quad (16)$$

The N to P stoichiometry of the fluxes across the sediment–water interface, $J_{N:P}$, can thus be calculated as:

$$J_{N:P} = J_{DIN}/J_{PO4} \quad (17)$$

Note that $J_{N:P}$ is not defined as J_{NO3}/J_{PO4} since the NH_4^+ released from the sediment will be rapidly oxidized to NO_3^- in the water column and it is the net flux of fixed N that is of most interest to global biogeochemical modelers. The molar N:C and C:P ratios of the fluxes (excluding the benthic C flux associated with the dissolution of $CaCO_3$) are:

$$J_{N:C} = J_{DIN}/C_{ox} \quad (18)$$

$$J_{C:P} = C_{ox}/J_{PO4} = r_{REG} \quad (19)$$

These metrics are used in this study to assess the stoichiometry and global distribution of benthic N and P fluxes.

4. Global Application of New Transfer Functions

4.1. Global Data Sets

[16] In addition to the site-specific data previously used to derive the transfer functions, global maps of bottom water O_2 and NO_3^- concentrations and RRPOC are needed to apply these functions at a global scale. O_2 and NO_3^- concentrations were obtained from annual objectively analyzed mean concentrations from the WOA 2005 [*Garcia et al.*, 2006a; 2006b] with a 1° × 1° horizontal resolution. These data were available for water depths up to 5500 m with a vertical resolution varying from 10 m close to the sea surface to 500 m for water depths >2000 m. The annual mean data recorded at the deepest water depth for a specific coordinate is assumed to be representative of the bottom water concentration.

[17] RRPOC (Figure 4a) were estimated from primary production data as follows. Mean monthly primary production rates were derived from satellite imagery of chlorophyll a (Chl a), photosynthetically available radiation (PAR) and sea–surface temperature (SST) following *Behrenfeld and Falkowski* [1997]. Monthly climatological data (1997–2010) for Chl a and PAR were obtained by SeaWIFS (G. C. Feldman and C. R. McClain, Ocean Color Web, SeaWIFS Reprocessing 5, 2010, http://oceancolor.gsfc.nasa.gov/), and monthly objectively analyzed means of SST were derived from the WOA 2005 [*Locarnini et al.*, 2006]. Based on the spatially resolved monthly primary production estimates, POC export production at each grid point was then determined using the pe-ratio [*Dunne et al.*, 2005]. Particle transport to the seafloor was subsequently calculated using the Martin curve [*Martin et al.*, 1987]:

$$RRPOC = F_{100} \times (z/100)^b \quad (20)$$

where RRPOC is the POC flux reaching the seafloor (mmol C m^{-2} d^{-1}), F_{100} is the POC flux at 100 m; assumed to be equal to the POC export production, and z is water depth (m). The value of the exponent (b = −0.82) was defined according to *Berelson* [2001], and is discussed in more detail later. The bathymetry of the seafloor was defined according to ETOPO5 [*Sloss*, 1988]. Finally, monthly RRPOC data calculated using equation (20) were integrated to give annual estimates.

[18] All data in the figures presented were processed on a 1° × 1° grid. Data available at higher resolution (SeaWIFS data at 9 × 9 km, bathymetry at 5′ × 5′) were averaged within each 1° × 1° grid cell. Upscaling of areal rates to total global fluxes (in Tg yr^{-1}) was achieved using the area of each 1° × 1° grid given by the NASA ISLSCP GDSLAM database [*Meeson et al.*, 1995]. For the calculation of globally-resolved J_{NO3}, J_{DIN} and J_{PO4} (Section 3.3), C_{ox} was determined by substituting the RRPOC estimated derived using Eq. (20) into Eq. (1) and (2).

4.2. Application of the Transfer Functions and Comparison With Previous Work

[19] Global maps of total benthic NO_3^- losses (L_{NO3} = maximum denitrification rate) and denitrification predict broad areas with high rates on the continental shelf of northern Russia, Europe, North America, Argentina and the East China Sea (Figure 5). Predicted rates were much lower at greater water depths, especially in the deep ocean basins. The distribution of denitrification using the two estimates (DEN1 and DEN2) were very similar and only DEN1 is shown in the figure. At eight grid points, denitrification rates of up to 13 mmol N m^{-2} d^{-1} were predicted, although for illustrative purposes the upper limit of the scale in Figures 5b and 5c was set to 5 mmol N m^{-2} d^{-1}. These maximum rates were found for the oxygen deficient waters off the Oregon coast (13 mmol N m^{-2} d^{-1}), Pakistan (11.7 mmol N m^{-2} d^{-1}), Namibia (8.8 mmol N m^{-2} d^{-1}), Mexico (7.6 mmol N m^{-2} d^{-1}), the Red Sea (6.9 mmol N m^{-2} d^{-1}) and Peru (5.9 mmol N m^{-2} d^{-1}). Although these areas generally exhibit high

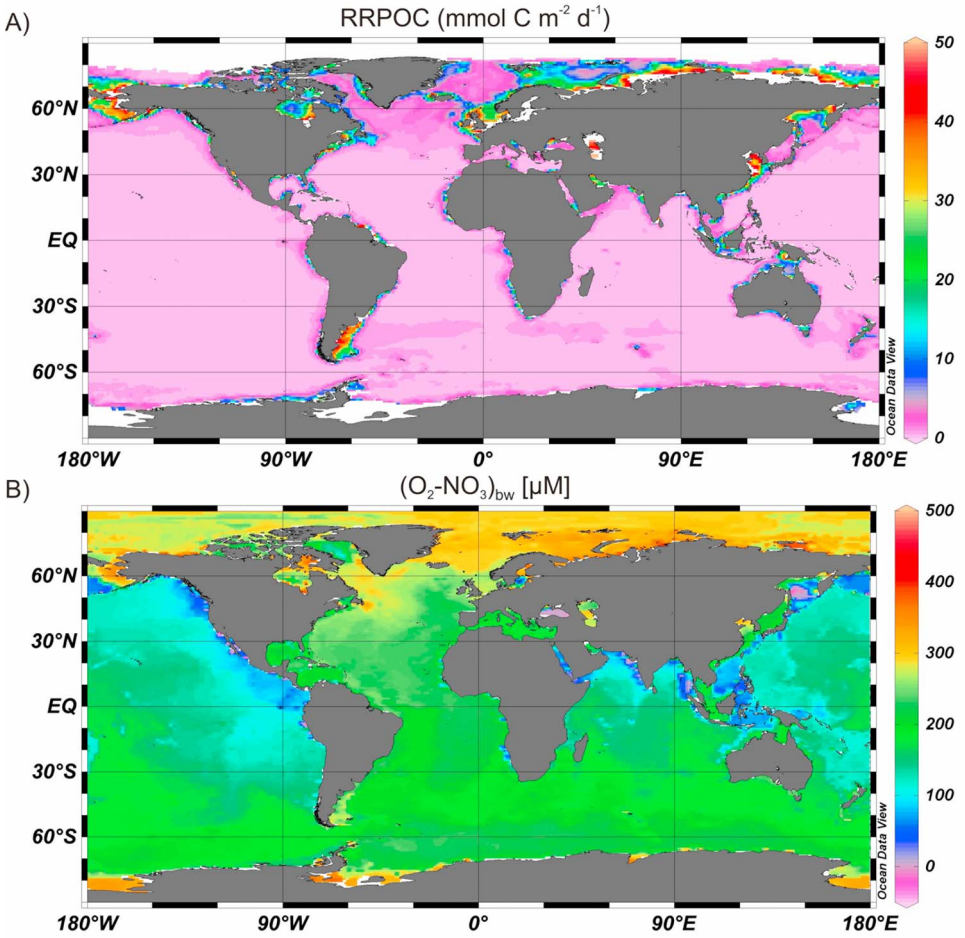

Figure 4. Global data sets on a 1° × 1° horizontal resolution. (a) POC rain rates (mmol C m^{-2} d^{-1}), calculated from primary production estimates (see section 4.1). (b) $(O_2\text{-}NO_3)_{bw}$ (μM).

denitrification rates, they are not always obvious on the figure because of the narrow continental shelves there. For comparison, measured rates are <4.7 mmol N m^{-2} d^{-1} for the Washington shelf close to the Oregon coast, <3.8 mmol N m^{-2} d^{-1} for the Pakistan margin and <2 mmol N m^{-2} d^{-1} for the Peru margin [*Bohlen et al.*, 2011; *Devol and Christensen*, 1993; *Schwartz et al.*, 2009]. These are a factor of 2 to 3 lower than our maximum values, which may be attributed to spatial heterogeneities or uncertainty in the rain rate (see below). An additional denitrification hot spot is predicted for the Gulf of California, yet to our knowledge no denitrification measurements are available for comparison. Nevertheless, the rain rates predicted for Guaymas Basin in the central Gulf of California are 3.4 mmol m^{-2} d^{-1} which is in the range reported by [*Thunell*, 1998] at the same location (0.2–4.2 mmol m^{-2} d^{-1}). This area is known as an anoxic site [e.g., *Roden*, 1958] and is thus most likely a location with high rates of NO_3^- loss based on our current understanding of N losses in HNLO environments [*Middelburg et al.*, 1996; *Bohlen et al.*, 2011]. Overall, our results emphasize the importance of HNLO/OMZ environments as areas of intense benthic denitrification.

[20] Denitrification rates in shelf, slope, and deep sea sediments are presented in Table 1 alongside globally–integrated rates. The model predicts that marine sediments consume 196 ± 33 Tg yr^{-1} of NO_3^- (L_{NO3}), of which more than half occurs on the continental shelf. After correcting for the NH_4^+ release, the globally integrated rate of denitrification amounts to 153 ± 40 Tg N yr^{-1} and 155 ± 67 Tg N yr^{-1} for DEN1 and DEN2, respectively. These very similar estimates corroborate the *a posteriori* approach that the NH_4^+ efflux is equal to ca. 27% of the NO_3^- influx for water depths <1000 m (section 3.2). More than 50% of denitrification takes place on the shelf despite the relatively small surface area (6% of total). This contribution is higher than the values predicted by the reaction–transport model approaches of *Middelburg et al.* [1996] (35–44%) and *Thullner et al.* [2009] (29%), most likely because of differences in the parameterization of the function describing the organic carbon rain rate to the seafloor. Despite very low denitrification rates in the deep sea (Figure 5), it contributes roughly 20% to the global rate owing to the large expanse of the deep ocean basins.

[21] Our benthic denitrification rates are well within the range of previously published estimates (Table 2).

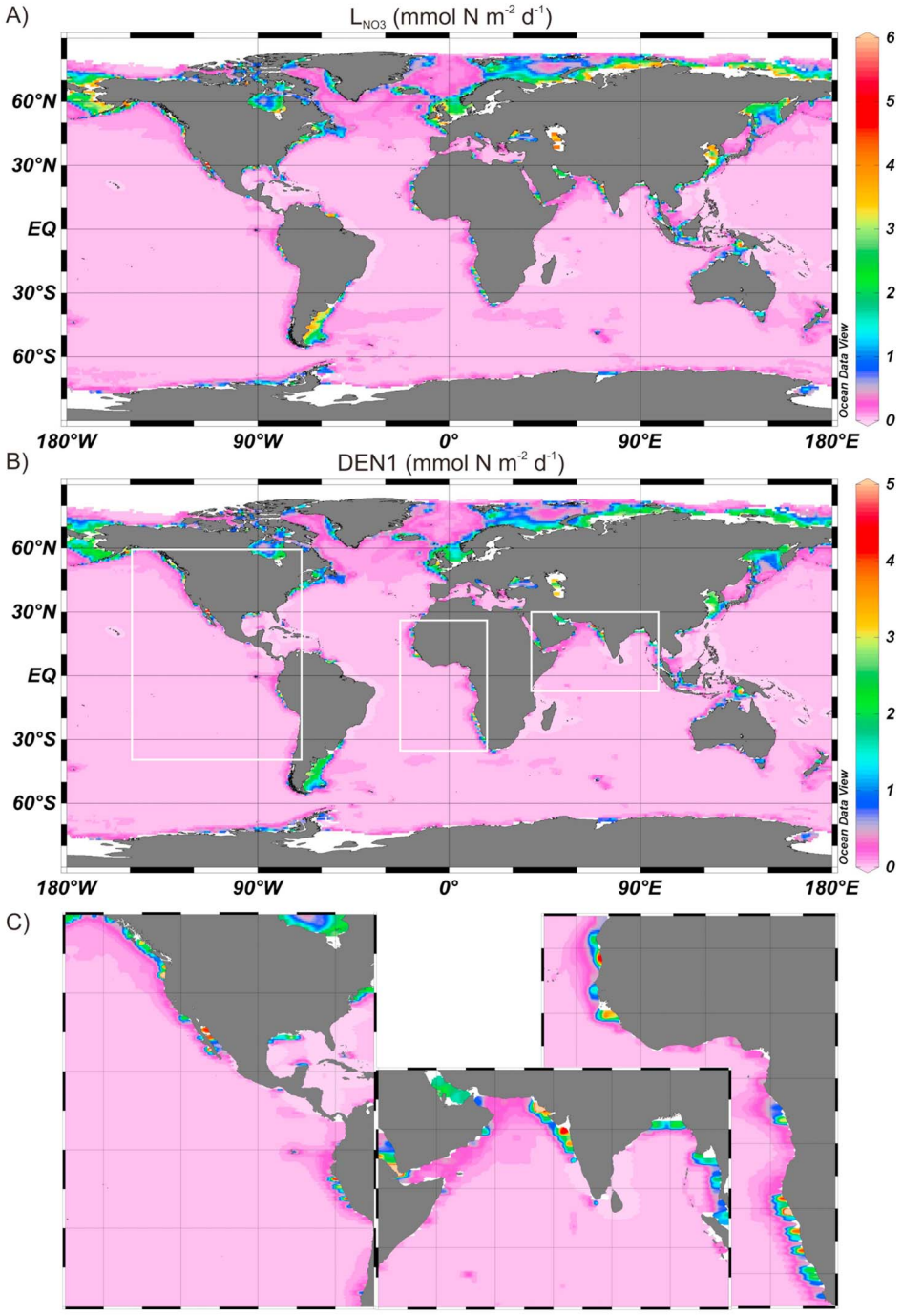

Figure 5. (a) Global maps of the predicted NO_3^- loss (L_{NO3}, mmol N m^{-2} d^{-1}); (b) *a priori* benthic denitrification estimate (DEN1, mmol N m^{-2} d^{-1}); (c) enlargements of DEN1 in major HNLO regions. For clarity the scale was set to a limit of 6 and 5 mmol N m^{-2} d^{-1} for L_{NO3} and DEN1, respectively, although higher rates were predicted for a limited number of grid points (see text).

Consequently, coupling of the transfer function (equation (10)) to global circulation models should provide a realistic estimate of regional variations in benthic denitrification. Importantly, since our approach implicitly includes anammox, our findings show that the relatively recent discovery of anammox in marine sediments likely does not require the present estimates the global benthic marine N budget to be revised [e.g., *Brandes et al.*, 2007; *Thamdrup and Dalsgaard*, 2002]. The rates reported by *Deutsch et al.* [2004], *Gruber* [2004], and *Thullner et al.* [2009] are more similar to ours than the estimates by *Middelburg et al.* [1996], *Codispoti et al.* [2001], *Brandes and Devol* [2002], and *Seitzinger et al.* [2006] which are up to ca. 2

Table 1. Mean Rates and Fluxes (Tg yr^{-1}) as Well as Atomic N:P, N:C, and C:P Ratios of the Fluxes[a]

	L_{NO3}	DEN1	DEN2[b]	RRPOC	J_{NO3}	J_{DIN}	J_{PO4}	$J_{N:P}$[c,d]	$J_{N:C}$[c,d]	$J_{C:P}$[d]
shelf (200 m, 6%)	110 ± 17 (56%)	84 ± 21 (55%)	80 ± 42 (52%)	1056 (60%)	4.3 (19%)	30.0 (50%)	13.8 (52%)	5.5	0.044	122.7
slope (200–2000 m, 10%)	51 ± 10 (26%)	41 ± 11 (27%)	40 ± 19 (26%)	393 (22%)	−4.9	5.0 (8%)	6.1 (23%)	4.3	0.031	121.7
deep sea (>2000 m, 84%)	35 ± 6 (18%)	28 ± 8 (18%)	35 ± 6 (22%)	312 (18%)	18.7 (81%)	25.5 (42%)	6.6 (25%)	9.0	0.073	122.6
global	196 ± 33	153 ± 40	155 ± 67	1761	18.1	60.5	26.5	8.3	0.067	122.4
<50 μM $bw_{O2\text{-}NO3}$ (1%)	18 ± 4 (9%)	16 ± 5 (11%)	14 ± 7 (9%)	61 (4%)	−11	−8.8	0.7 (3%)	−10.9	−0.13	93

[a]Negative NO_3^- fluxes indicate uptake by the sediment. Percentages of global seafloor area, effluxes, and rates are given in parentheses.

[b]$\Delta DEN2 = \begin{cases} \Delta L_{NO3} + 0.23 \times L_{NO3} & \text{for water depths} < 1000\text{ m} \\ \Delta L_{NO3} & \text{for water depths} > 1000\text{ m} \end{cases}$ (23% error in *aposteriori* correction of NH_4^+ *for* < 1000 m)

[c]N = DIN

[d]The stoichiometry of the fluxes is calculated as the average of sum of the values from the individual grid cells.

times higher. The value obtained by *Archer et al.* [2002] is an order-of-magnitude greater than ours (1960 Tg N y^{-1}), which may be due to their extrapolation procedure which is based on bathymetry rather than biogeochemical gradients.

[22] The first systematic study estimating global denitrification in sediments was carried out by *Middelburg et al.* [1996] using a 1-D diagenetic model constrained by measured pore water concentrations and fluxes from different marine settings. By varying bottom water O_2 and NO_3^- concentrations and rain rates over realistic ranges, these authors derived a semi–empirical transfer function ('meta-model') to predict benthic denitrification as a function of these variables and water depth. Their globally integrated denitrification rates of 230–285 Tg N yr^{-1} (Table 2) are around 70% higher than ours. This discrepancy is rooted in the 76% higher rain rate used by these workers (1761 c.f. 3094 Tg C yr^{-1}; Table 2). In fact, Middelburg's model yields a much closer value of 170 Tg N yr^{-1} for our global carbon flux of 1761 Tg C (J. Middelburg, personal communication, 2012). Thus, the modeling based meta-model and the empirically derived transfer functions demonstrate a high degree of coherency.

[23] Because most of the studies listed in Table 2 employ a variety of simplifications and averaging procedures, the spatial distribution of benthic denitrification remains poorly understood. *Seitzinger et al.* [2006] provide a global map for denitrification in continental shelf and OMZ regions which highly resembles the distribution in this study, although their denitrification estimate for continental shelf sediments is 62% higher (Table 2). Moreover, a recent study by *Somes et al.* [2010] using a general circulation model reports similar hot spots of benthic denitrification as our findings, yet with distinctively lower maximum rates (≤2.7 mmol N m^{-2} d^{-1}) and much lower globally–integrated rates (38.2 Tg N yr^{-1}). These workers calculated benthic denitrification based on the labile organic carbon flux to the seafloor from the parameterization by *Middelburg et al.* [1996]. Since the function developed by these authors yields rates which are of the same order of magnitude as ours, differences in rain rate (i.e., productivity) are most likely the reason for the discrepancy with the estimate of *Somes et al.* [2010]. In fact, because denitrification scales linearly with the rain rate, the spatial distribution of denitrification (Figure 5) and rain rate (Figure 4a) is very similar.

[24] The shape of the curves in Figures 3a and 3d shows that the effect of bottom water chemistry on denitrification becomes more important at low or negative values of $(O_2\text{-}NO_3)_{bw}$, that is, in HNLO settings. Most of the oceanic bottom waters are characterized by $(O_2\text{-}NO_3)_{bw}$ values in excess of 150 μM. Oxygen minimum zones are extreme examples of HNLO environments yet they impinge on only ca. 1% of the seafloor (defined as <0.5 ml l^{-1} O_2 [*Helly and Levin*, 2004] or $(O_2\text{-}NO_3)_{bw} \approx 50$ μM, Table 1). Nevertheless, OMZs accounted for around 10% of the total benthic denitrification rate (Table 1). When normalized to surface area, OMZ and shelf sediments are clearly seen to be key regions for benthic denitrification (Figure 6). The figure further demonstrates that denitrification in shelf, slope and deep-sea sediments accounts for roughly 10% of the rain rate in agreement with model results by *Middelburg et al.* [1996]. However, OMZs sediments denitrify on average 3 times as much NO_3^- per area as normal oxic shelves due to the HNLO

Table 2. Comparison of Published Denitrification Rates (L_{DIN}) and Organic Carbon Rain Rates (Tg yr^{-1}) Listed From Highest to Lowest

Parameter	Value	Reference	Method
denitrification (global)	1960	*Archer et al.* [2002]	reaction–transport model
	300	*Codispoti et al.* [2001]	data extrapolation and interpretation
	230 – 285	*Middelburg et al.* [1996]	reaction–transport model
	200 – 280	*Brandes and Devol* [2002]	N isotope budget
	250[a]	*Seitzinger et al.* [2006]	model based on depth–integrated water column primary production (PP)
	190	*Deutsch et al.* [2004]	N isotope box model
	180 ± 50	*Gruber* [2004]	data extrapolation and interpretation
	153 – 155	This study	
	154	*Thullner et al.* [2009]	reaction–transport model
	88[b] – 115[c]	*Romaniello and Derry* [2010]	intermediate–complexity box model
	38.2	*Somes et al.* [2010]	global circulation model
RRPOC (global)	3094[d]	*Middelburg et al.* [1997]	empirical function based on water depth
	2300, 2628[e]	*Burdige* [2007]	global compilation of organic matter remineralization rates
	2290 ± 900	*Dunne et al.* [2007]	satellite PP estimate plus series of conversion functions (see text)
	1761	This study	
	930	*Muller-Karger et al.* [2005]	satellite PP estimate plus empirical settling function
RRPOC shelf and slope (<2000 m)	1980 (86%)	*Dunne et al.* [2007]	satellite PP estimate plus series of conversion functions (see text)
	1684, 2013 (73%, 77%)[e]	*Burdige* [2007]	global compilation of organic matter remineralization rates
	1449 (82%)	This study	
	620 (67%)	*Muller-Karger et al.* [2005]	satellite PP estimate plus empirical settling function
RRPOC deep sea (>2000 m)	616 (27%, 23%)[e]	*Burdige* [2007]	global compilation of organic matter remineralization rates
	312 (18%)	This study	
	310 (33%)	*Muller-Karger et al.* [2005]	satellite PP estimate plus empirical settling function
	310 (14%)	*Dunne et al.* [2007]	satellite PP estimate plus series of conversion functions (see text)

[a]Continental shelf only.
[b]Intermediate-complexity box model with 79 boxes.
[c]Intermediate-complexity box model with 13 boxes.
[d]Labile organic carbon flux calculated as described by *Middelburg et al.* [1996] with the bathymetric grid used in this study (see section 4.1).
[e]From sediment organic carbon budget with and without accounting for relict sand on the continental shelf, respectively.

conditions established there. Denitrification is predicted to account for up to 50% of carbon respired in extreme cases, which is in line with previous results [*Burdige*, 2006; *Bohlen et al.*, 2011]. In general, the global geographical distribution of denitrification can mainly be explained by the rain rate of organic carbon throughout much of the ocean except for HNLO environments where the $(O_2\text{-}NO_3)_{bw}$ term dominates. Similar findings have been described by *Fennel et al.* [2009] who noted that sediment oxygen consumption (i.e., C_{ox}) and the J_{NO3} were the most effective predictors of the denitrification rate. Interestingly, in their analysis they concluded that O_2 and NO_3^- concentrations were the least effective predictors when analyzed as part of a multiple regression. Our results suggest that the combination of these two variables is a much more powerful predictor of denitrification, since $(O_2\text{-}NO_3)_{bw}$ directly characterizes HNLO regions where rates are highest.

4.3. Dependency of N Losses on the Rain Rate

[25] The estimation of the benthic NO_3^- loss and denitrification includes uncertainties within the global data sets of bottom water O_2 and NO_3^- concentrations and the carbon rain rate. While bottom water chemistry is well known for most of the ocean, the accurate prediction of the rain rate is one of the most critical issues in ocean biogeochemistry and is associated with the most uncertainty. In general, the organic carbon flux to the seafloor may be quantified by two approaches: 'top-down' particle flux measurements using sediment traps and 'bottom-up' estimates based on measured benthic mineralization rates. Particle traps involve hydrodynamic effects, trapping of swimmers and solubilization of material once caught inside the trap [*Buesseler et al.*, 2007]. These problems are especially pronounced in the upper 1000 m of

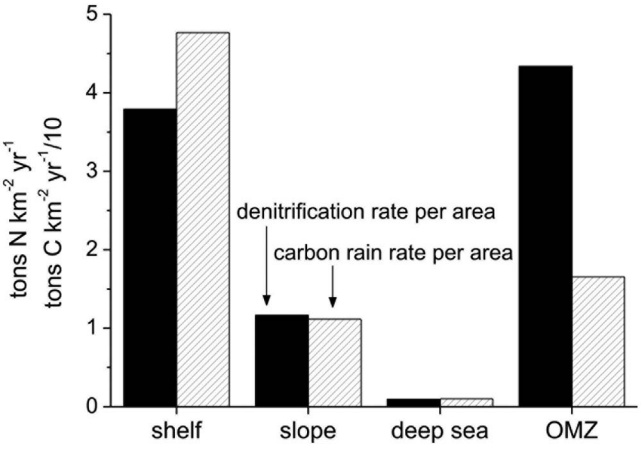

Figure 6. Denitrification rate per area (tons N km^{-2} yr^{-1}) and carbon rain rate per area (tons C km^{-2} yr^{-1} /10) for shelf, slope, deep sea and OMZ sediments.

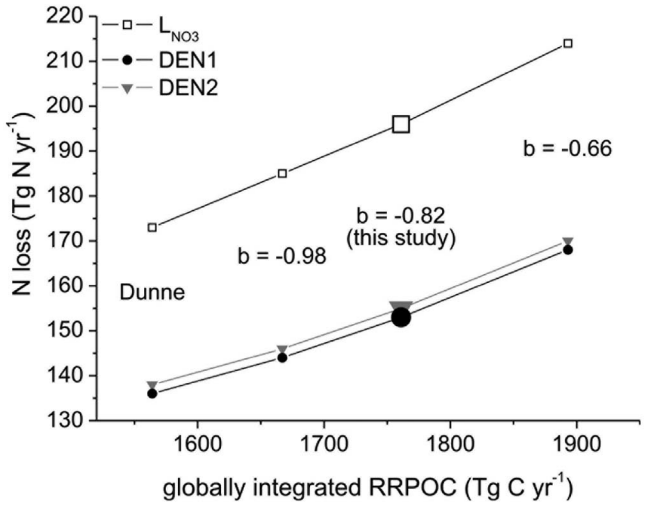

Figure 7. Globally integrated benthic NO_3^- losses and denitrification rates (DEN1 and DEN2) as a function of carbon rain rate (RRPOC). RRPOC for <2000 m water depth were calculated with different values of the Martin curve exponent, b, and following *Dunne et al.* [2007] while RRPOC for >2000 m water depth are the same as the standard run (b = −0.82). The values used in this study are indicated with larger symbols.

the water column where lateral flows are stronger and the abundance of swimmers is higher. With regard to bottom-up approaches, benthic degradation rate estimates may have to be corrected for organic carbon burial which is itself a large source of uncertainty [e.g., *Jahnke*, 1996]. Furthermore, the seafloor is dramatically undersampled which creates large uncertainties for regional upscaling.

[26] In this study, rain rates were estimated using the 'Martin curve' [*Martin et al.*, 1987], a function based on sediment trap data, with an exponent b = −0.82. This exponent is a mean value derived from particle flux measurements at 17 U.S. JGOFS stations [*Berelson*, 2001]. In fact, the Martin curve exponent may vary substantially between regions [*Martin et al.*, 1987; *Berelson*, 2001] and the use of a single exponent in global extrapolations may be a gross oversimplification. The Martin curve may also not hold for suboxic waters. The original work by *Martin et al.* [1987] and a more recent study by *Van Mooy et al.* [2002] imply exponents of −0.3 to −0.4 for oxygen-deficient waters, that is, more carbon reaches to the seafloor at these sites. Average rain rates estimated for the Peruvian OMZ at 11°S calculated using the approach in this study are 8.9 mmol m^{-2} d^{-1} compared to 9.6 mmol m^{-2} d^{-1} estimated from individual sediment mass balances at 6 stations at the same location [*Bohlen et al.*, 2011]. Thus, although top-down and bottom-up approaches yield similar carbon rain rates for this location, it may not do so for other OMZs.

[27] Despite these uncertainties, our globally integrated rain rate and distribution are similar to those previously reported although there is much work to do to refine these numbers (Table 2). Since the shelf and slope are the main regions for benthic denitrification, the variability in rain rate for water depths <2000 m is of most significance globally. Accordingly, we tested the sensitivity of RRPOC to different values of the Martin curve exponent, b. L_{NO3} and denitrification were recalculated applying the standard deviation in b (b = −0.82 ± 0.16) reported by *Berelson* [2001]. Furthermore, we also tested the Martin curve used by *Dunne et al.* [2007], who estimated the POC rain rate based on the export out of the 75 m depth horizon with b = −0.9, i.e., $RRPOC = F_{75} \times (z/75)^{-0.9}$. Global fields for RRPOC using the 3 additional b values were derived for water depths <2000 m and complimented with RRPOC data from the standard run with b = −0.82. New globally integrated RRPOC ranged from 1564 Tg C yr^{-1} when applying the Martin curve used in *Dunne et al.* [2007] to 1893 Tg C yr^{-1} for an exponent of −0.66 (Figure 7). This changes the estimate for global NO_3^- loss and denitrification rate by ±23 and ±17 Tg N yr^{-1}, respectively. In relative terms, these differences roughly equate to a change of 11%, which demonstrates that the error in the global benthic NO_3^- loss and denitrification estimates scales with the uncertainty in the rain rate. Consequently, our global benthic N losses are accurate to the same order as the rain rate.

4.4. Enhanced N Loss in Sandy Sediments?

[28] The transfer functions are mainly derived from data gathered from muddy sediments. Coarser–grained shelves are not as well represented in the database, probably due to sampling difficulties and hard-to-determine transport pathways for solutes [e.g., *Huettel and Rusch*, 2000; *Jahnke et al.*, 2005]. Nonetheless, up to 70% of the shelf is covered with non-accumulating relict sands with low organic carbon content [*Emery*, 1968]. Some reports suggest that denitrification rates in such settings could be lower, yet still significant, than those in fine-grained sediments [*Vance-Harris and Ingall*, 2005]. Other studies claim that sandy shelves are important sites for organic matter mineralization due to efficient ventilation of surface sands by advective processes [e.g., *Huettel and Rusch*, 2000; *Rao et al.*, 2007]. In global terms, the denitrification estimate by *Brandes and Devol* [2002] based on an isotopic mass balance, and therefore inclusive of all sediment types, yields rates which are 30–80% higher than those obtained in our approach (Table 2). This discrepancy may indeed allude to high rates of denitrification in sandy sediments or reflect the uncertainty associated with the two very different approaches. The magnitude of denitrification in sandy sediments requires urgent attention, especially since our study indicates areas of high N loss rates in regions where sandy sediments are common such as the continental slope off Argentina (Figure 5). Estimates at such locations are thus subject to greater uncertainty. The range of estimates in Table 2 illustrates that there is still much room for refining global benthic denitrification rates, and more data from sandy shelf sediments is required to resolve their importance as sites of fixed N loss.

4.5. Benthic N and P Fluxes

[29] The geographical distribution of the benthic NO_3^- and net DIN fluxes are shown in Figures 8a and 8b. In the deep-sea areas, the fluxes were close to zero due to low organic matter degradation rates and the dominance of aerobic respiration [e.g., *Thullner et al.*, 2009]. As expected, maximum uptake rates into the sediment were associated with the OMZ regions (Oregon, Pakistan, Namibia, Mexico, Red Sea, Peru)

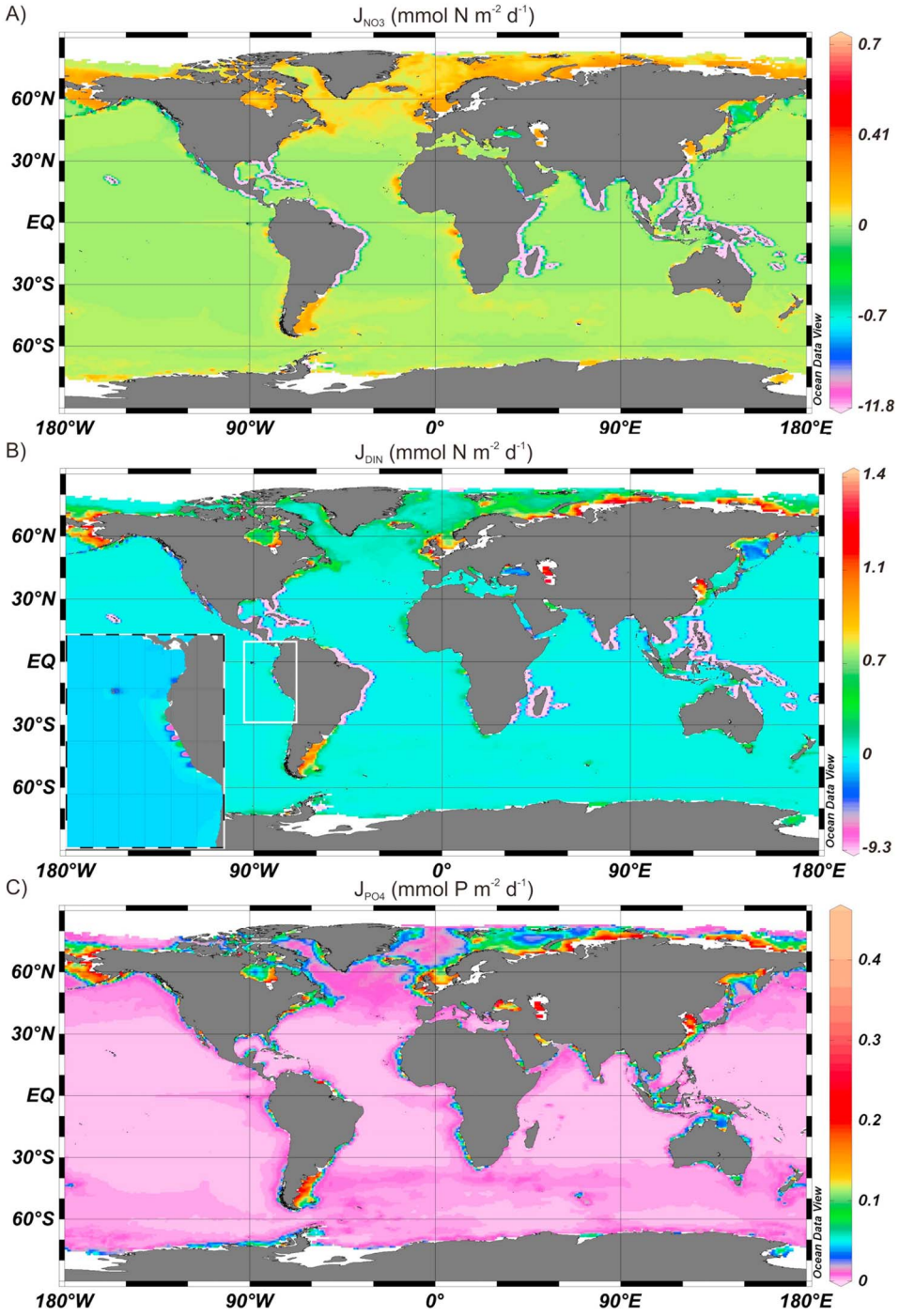

Figure 8. Global map of the predicted (a) nitrate (J_{NO3}), (b) DIN (J_{DIN}), and (c) phosphate (J_{PO4}) benthic fluxes in mmol m^{-2} d^{-1}. The inset in Figure 8b shows an enlargement of J_{DIN} for the Peruvian margin. Note the non–linear scales in Figures 8a and 8b.

with J_{NO3} and J_{DIN} approaching −12 and −9 mmol N m^{-2} d^{-1}, respectively, for the Oregon shelf. Uptake of NO_3^- and DIN was predicted for all locations with low $(O_2\text{-}NO_3)_{bw}$. High effluxes of NO_3^- (≤0.3 mmol m^{-2} d^{-1}) and DIN (≤1.4 mmol m^{-2} d^{-1}) were mainly restricted to the high latitude continental shelves and the Argentine Basin, most likely due to high rates of nitrification of NH_4^+ released from organic nitrogen as *Hensen et al.* [1998] have shown. Interestingly, for the coastal OMZs offshore Peru and West Africa, sites with net DIN uptake and release in close proximity are predicted, as exemplified by the enlargement of the Peruvian OMZ in Figure 8b. Regime shifts in benthic N cycling dominated by denitrification (DIN sink) and DNRA (DIN recycling) have been shown to be consistent with such

features along a transect of the Peruvian OMZ at 11°S [*Bohlen et al.*, 2011].

[30] For the global ocean, the transfer function yielded a total benthic DIN release of 60.5 Tg N yr^{-1} (Table 1). The shelf contributed 50% to this flux, followed by the deep sea with 42% and the slope with only 8%. A comparison with J_{NO3} shows that the efflux of DIN was dominated by NO_3^- rather than NH_4^+ in the deep sea. In contrast, the large difference between J_{NO3} and J_{DIN} on the shelf shows that NH_4^+ release from organic matter and, potentially, DNRA supports most of the DIN efflux here.

[31] A net global NO_3^- release rate of 18.1 Tg N yr^{-1} was estimated due to the contribution of shelf and deep-sea sediments that act as NO_3^- sources due to nitrification [*Middelburg et al.*, 1996]. The model predicted a net uptake of nitrate of −4.9 Tg N yr^{-1} on the slope where the HNLO regions impinge on the seafloor (<50 μM $(O_2\text{-}NO_3)_{bw}$). The importance of HNLO areas as global NO_3^- sinks is demonstrated by their removal of 11 Tg N yr^{-1}, equivalent to 61% of the total benthic flux NO_3^- input (Table 1).

[32] The distribution of benthic PO_4^{3-} effluxes (Figure 8c) based on the algorithm of *Wallmann* [2010] was similar to that for NO_3^- and the rain rate (Figure 4a), that is, low fluxes in the deep sea basins and higher fluxes on the Arctic shelf, Argentine Basin and OMZs. The globally integrated PO_4^{3-} flux was estimated to be 26.5 Tg P yr^{-1}, mainly due to release from shelf sediments (Table 1). This is comparable with the pre-anthropogenic global benthic release of 33 Tg P yr^{-1} derived by *Wallmann* [2010].

4.6. Benthic C:N:P Regeneration Ratios

[33] The atomic N:P ($J_{N:P}$), N:C ($J_{N:C}$) and C:P ($J_{C:P}$) ratios of the benthic exchange flux between sediments and seawater are shown globally in Figure 9. The values of $J_{N:P}$, $J_{N:C}$ and $J_{C:P}$ expected from Redfield are 16, 0.15 and 106, respectively [*Redfield et al.*, 1963].

[34] On the continental shelf the mean $J_{N:P}$ was very low (5.5) despite the net DIN release, while in the deep sea where nitrification was most prevalent the ratio was higher (9.0) but still below Redfield (Table 1). For HNLO regions, a negative N:P ratio was calculated as a result of net DIN uptake, illustrating extreme non-Redfield flux stoichiometry when $(O_2\text{-}NO_3)_{bw}$ falls below ca. 100 μM. In general, low $J_{N:P}$ were associated with HNLO environments (Figure 9a), a feature that has already been observed previously [*Hartnett and Devol*, 2003]. These workers reported average N:P ratios of 2.9 and 10.6 (considering NH_4^+ fluxes only) for the oxygen deficient margins of northwest Mexico and Washington, respectively. The globally–averaged $J_{N:P}$ of the benthic fluxes was 8.3 (Table 1), which takes into account NO_3^- uptake by the sediments on the slope. This value, and even the maximum predicted ratio of 10.9 (Figure 9a), is much lower than the Redfield value of 16 [*Redfield et al.*, 1963; *Anderson*, 1995]. These findings strikingly demonstrate that the major ocean basins release nutrients to the bottom water in a highly non-Redfield composition, implying either a loss of DIN relative to PO_4^{3-} or enhanced release of PO_4^{3-}.

[35] Values for $J_{N:C}$ were positive for most of the seafloor due to DIN release (Figure 9b). Nonetheless, the globally averaged $J_{N:C}$ of 0.067 is a factor of 2 – 3 lower than Redfield (0.151), and a factor of 2 lower than the revised N:C phytoplankton composition of 0.137 [*Anderson and Sarmiento*, 1994]. The fluxes of solutes from shelf, slope and deep sea sediments are deficient in N relative to C (and P). Therefore, the low $J_{N:P}$ throughout the ocean discussed in the previous paragraph is due to preferential N loss rather than excess P release (see also following paragraph). *Hartnett and Devol* [2003] also measured lower N:C ratios (NH_4^+ fluxes considered only) than Redfield with average values of 0.093 and 0.039 for the oxygen-deficient environments off Mexico and the Washington margin, respectively. By comparison, our OMZ estimate for $J_{N:C}$ is high and negative (−0.13) because it considers both NO_3^- and NH_4^+, and again demonstrates the strong sink for DIN in HNLO settings.

[36] The global distribution of $J_{C:P}$ (Figure 9c) shows that, for most regions of the ocean, carbon-to-phosphate flux ratios were higher than predicted by Redfield. The same applies to the shelf, slope, deep sea and global averages (Table 1). The oceans are generally well-ventilated and C:P ratios up to 123:1 are expected for high bottom water O_2 concentrations [*Wallmann*, 2010], which indicates preferential burial of phosphorus and P–limiting fluxes with regards to C. However, some individual locations such as the Peruvian and Pakistani OMZs or the Black Sea had considerably lower $J_{C:P}$ with a minimum of 13. Such low C:P regeneration ratios in shelf sediments are believed to result from massive excess P release under low-oxygen conditions due to the reductive dissolution of P-adsorbed manganese and iron oxyhydroxides and the preferential degradation of particulate organic P in anoxic sediments [e.g., *Ingall and Jahnke*, 1994]. Consequently, and as expected from equation (15), the C:P regeneration ratio decreases on eastern boundaries where bottom water O_2 concentrations are diminished (Figure 9c). The value of $(O_2\text{-}NO_3)_{bw}$ where $J_{C:P}$ falls below Redfield is predicted to be around 20 μM. At this concentration, sediments become net sources of excess phosphate while acting as strong sinks for fixed N.

[37] To our knowledge, the impact of highly non-Redfield C:N:P mineralization ratios and benthic fluxes on oceanic nutrient cycles has yet to be evaluated in global models which typically assume Redfield mineralization, with few exceptions [e.g., *Somes et al.*, 2010]. The preferential burial of P in deep-sea sediments, the release of P in HNLO regions and the drawdown of fixed N globally will feedback on the simulation of nutrient distributions in global models integrated over time-scales on the order or larger than the oceanic residence time of N (<3000 yrs) [*Gruber and Sarmiento*, 1997; *Brandes and Devol*, 2002] and P (30,000 to 50,000 years) [*Delaney*, 1998]. A quantitative description of how sediment processes affect the distribution of conservative tracers, such as N* [*Gruber and Sarmiento*, 1997], in the modern ocean is not trivial to provide at this stage and will require analysis using global circulation models. This is especially true for shallower sediments on the shelf and slope of HNLO regions where the sediments will have the most impact on water column distributions. Regional models in these systems should therefore incorporate benthic dynamics in future applications to test the significance of the benthos [e.g., *Koné et al.*, 2005; *Lachkar and Gruber*, 2011]. We hypothesize that proper consideration of the C:N:P efflux ratios from marine sediments in global models will lead to a

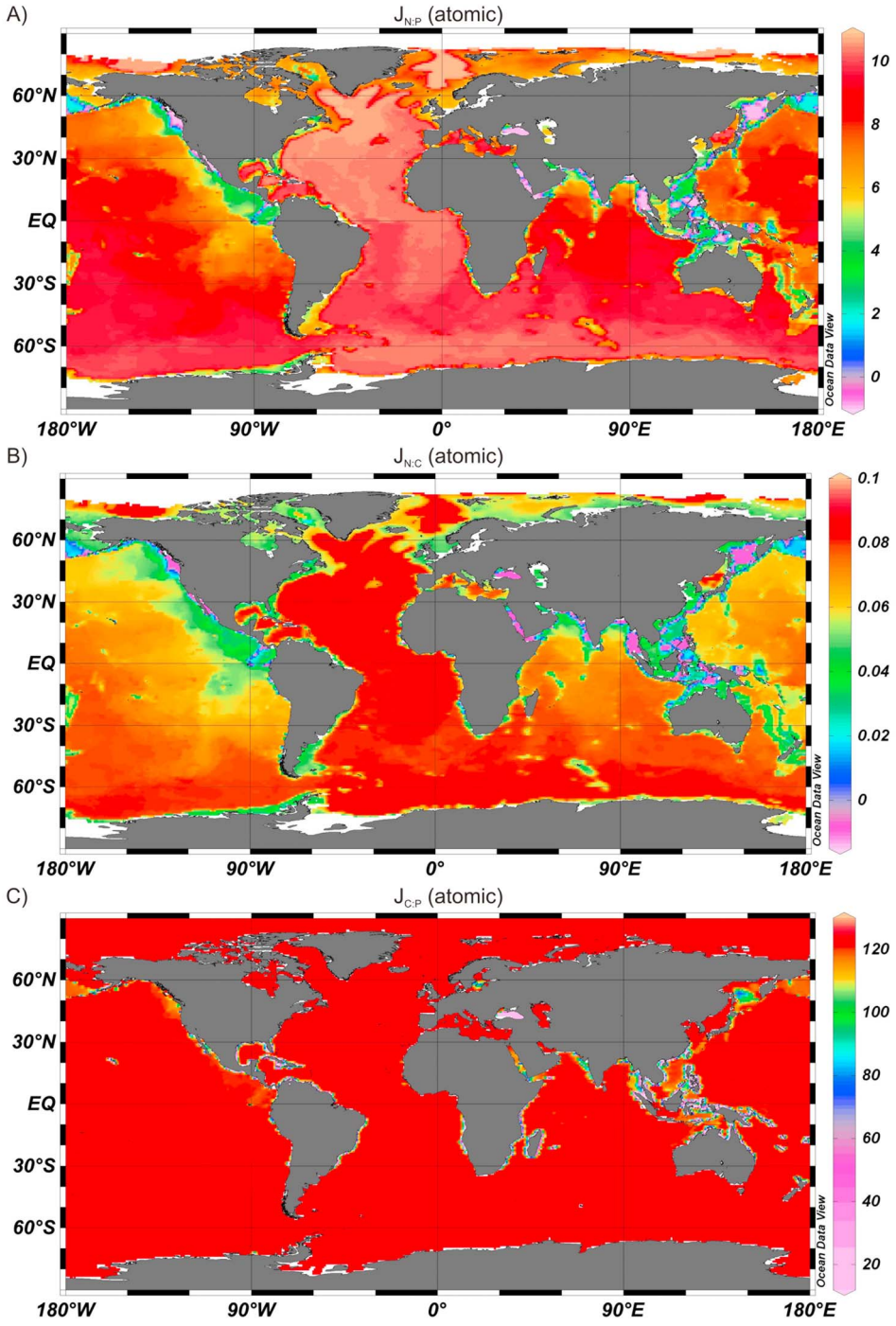

Figure 9. Global maps of the atomic (a) N:P ($J_{N:P}$), (b) N:C ($J_{N:C}$) and (c) C:P ($J_{C:P}$) ratios of the predicted fluxes. $J_{C:P}$ was calculated using the function derived by *Wallmann* [2010]. All negative ratios in Figures 9a and 9b are represented in pink. Note the nonlinear scaling in Figure 9b.

more accurate spatial description of both benthic and pelagic denitrification which presently reply on dissolved N and P distributions [*Sarmiento and Gruber*, 2006].

5. Conclusions

[38] A vertically integrated sediment model, or dynamic transfer function, is derived to calculate rates of benthic N loss by denitrification. The only input parameters required are the organic carbon rain rate and a newly proposed variable $(O_2\text{-}NO_3)_{bw}$; equivalent to the bottom water O_2 concentration minus that of NO_3^-. Low or negative $(O_2\text{-}NO_3)_{bw}$ thus indicate high-nitrate low-oxygen regions (HNLO) where denitrification rates are highest. Globally integrated benthic denitrification rates estimated when applying this transfer function to global databases of input variables yields

values of 153–155 Tg N yr^{-1}. These are well within the range of previously reported values. Importantly, this shows that the implicit inclusion of anammox in our approach does not enhance the magnitude of global N loss in marine sediments, implying that a significant revision of the sedimentary N sinks due to anammox is not required. Shelf sediments contributed >50% to the total N sink, followed by the slope (ca. 30%) and the deep sea (ca. 20%). Highest areal rates were found for the HNLO regions off Oregon, Pakistan, Namibia, Mexico, the Red Sea and Peru, as well as the high latitude oxic continental shelf. Despite only covering about 1% of the seafloor, sediments underlying HNLO settings remove around 3 times as much N per unit of carbon deposited and account for ca. 10% of global benthic denitrification. By applying a similar transfer function for predicting carbon-to-phosphorus regeneration ratios in marine sediments [*Wallmann*, 2010], a strong deviation from Redfield N:P, N:C, and C:P stoichiometric ratios of the benthic fluxes has been demonstrated for the entire ocean. Although, on average, P is preferentially buried, the loss of fixed N through denitrifying pathways is much more intense and widespread, resulting in N limitation of benthic fluxes with regard to both C and P.

[39] The transfer functions are based on empirical data. Therefore, although they sidestep the need for global parameterizations required for reaction-transport modeling approaches [e.g., *Thullner et al.*, 2009], they rely on a sufficiently large supporting database covering a broad range of marine environments. The present function meets these requirements although N cycling in sands is under-represented due to a lack of field observations. Our work has shown that the largest uncertainty is the rain rate of carbon to the seafloor, and differences between several independent global denitrification estimates can be largely attributed to this variable. The functions developed here are designed to be coupled easily to biogeochemical general circulation models which routinely employ organic carbon rain rates, nutrient and O_2 concentrations. Given the importance of benthic processes to N and P drawdown, we anticipate that global circulation models that account for these sinks will reveal new and exciting information on the importance of preferential nutrient mineralization during export and sinking of new production, the potential spreading of oxygen minimum zones and the scale of N limitation in the contemporary, past and future ocean.

[40] **Acknowledgments.** We are grateful to Jack Middelburg and an anonymous reviewer for their useful critique and suggestions that have improved the first version of this paper. This work is a contribution of the Sonderforschungsbereich 754 "Climate – Biogeochemistry Interactions in the Tropical Ocean" (www.sfb754.de) which is supported by the Deutsche Forschungsgemeinschaft.

References

Anderson, L. A. (1995), On the hydrogen and oxygen content of marine phytoplankton, *Deep Sea Res., Part I*, *42*(9), 1675–1680.

Anderson, L. A., and J. L. Sarmiento (1994), Redfield ratios of remineralization determined by nutrient data analysis, *Global Biogeochem. Cycles*, *8*(1), 65–80.

Andersson, J. H., J. W. M. Wijsman, P. M. J. Herman, J. J. Middelburg, K. Soetaert, and C. Heip (2004), Respiration patterns in the deep ocean, *Geophys. Res. Lett.*, *31*, L03304, doi:10.1029/2003GL018756.

Archer, D. E., J. L. Morford, and S. R. Emerson (2002), A model of suboxic sedimentary diagenesis suitable for automatic tuning and gridded global domains, *Global Biogeochem. Cycles*, *16*(1), 1017, doi:10.1029/2000GB001288.

Behrenfeld, M. J., and P. G. Falkowski (1997), Photosynthetic rates derived from satellite-based chlorophyll concentration, *Limnol. Oceanogr.*, *42*(1), 1–20.

Berelson, W. M. (2001), The flux of particulate organic carbon into the ocean interior: A comparison of four U.S. JGOFS regional studies, *Oceanography*, *14*, 59–67.

Bohlen, L., A. W. Dale, S. Sommer, T. Mosch, C. Hensen, A. Noffke, F. Scholz, and K. Wallmann (2011), Benthic nitrogen cycling traversing the Peruvian oxygen minimum zone, *Geochim. Cosmochim. Acta*, *75*, 6094–6111, doi:10.1016/j.gca.2011.08.010.

Brandes, J. A. and A. H. Devol (2002), A global marine-fixed nitrogen isotopic budget: Implications for holocene nitrogen cycling, *Global Biogeochem. Cycles*, *16*(4), 1120, doi:10.1029/2001GB001856.

Brandes, J. A., A. H. Devol, and C. Deutsch (2007), New developments in the marine nitrogen cycle, *Chem. Rev.*, *107*, 577–589, doi:10.1021/cr050377t.

Buesseler, K. O., et al. (2007), An assessment of the use of sediment traps for estimating upper ocean particle fluxes, *J. Mar. Res.*, *65*, 345–416.

Burdige, D. J. (2006), *Geochemistry of Marine Sediments*, Princeton Univ. Press, Princeton, N. J.

Burdige, D. J. (2007), Preservation of organic matter in marine sediments: Controls, mechanisms, and an imbalance in sediment organic carbon budgets?, *Chem. Rev.*, *107*(2), 467–485.

Christensen, J. P., J. W. Murray, A. H. Devol, and L. A. Codispoti (1987), Denitrification in continental shelf sediments has major impact on the oceanic nitrogen budget, *Global Biogeochem. Cycles*, *1*(2), 97–116, doi:10.1029/GB001i002p00097.

Codispoti, L. A., et al. (2001), The oceanic fixed nitrogen and nitrous oxide budgets: Moving targets as we enter the anthropocene?, *Sci. Mar.*, *65*, 85–105.

Codispoti, L. A., and J. P. Christensen (1985), Nitrification, denitrification and nitrous oxide cycling in the eastern Tropical South Pacific Ocean, *Mar. Chem.*, *16*(4), 277–300.

Dale, A. W., et al. (2011), Rates and regulation of nitrogen cycling in seasonally hypoxic sediments during winter (Boknis Eck, SW Baltic Sea): Sensitivity to environmental variables, *Estuarine Coastal Shelf Sci.*, *95*, 14–28, doi:10.1016/j.ecss.2011.05.016.

Dalsgaard, T., et al. (2005), Anaerobic ammonium oxidation (anammox) in the marine environment, *Rev. Microbiol.*, *156*, 457–464.

Delaney, M. L. (1998), Phosphorus accumulation in marine sediments and the oceanic phosphorus cycle, *Global Biogeochem. Cycles*, *12*(4), 563–572, doi:10.1029/98GB02263.

Deutsch, C., D. M. Sigman, R. C. Thunell, A. N. Meckler, and G. H. Haug (2004), Isotopic constraints on glacial/interglacial changes in the oceanic nitrogen budget, *Global Biogeochem. Cycles*, *18*, GB4012, doi:10.1029/2003GB002189.

Devol, A. H. (1991), Direct measurement of nitrogen gas fluxes from continental shelf sediments, *Nature*, *349*(6307), 319–321.

Devol, A. H., and J. P. Christensen (1993), Benthic fluxes and nitrogen cycling in sediments of the continental margin of the eastern North Pacific, *J. Mar. Res.*, *51*(2), 345–372.

Dunne, J. P., R. A. Armstrong, A. Gnanadesikan, and J. L. Sarmiento (2005), Empirical and mechanistic models for the particle export ratio, *Global Biogeochem. Cycles*, *19*, GB4026, doi:10.1029/2004GB002390.

Dunne, J. P., J. L. Sarmiento, and A. Gnanadesikan (2007), A synthesis of global particle export from the surface ocean and cycling through the ocean interior and on the seafloor, *Global Biogeochem. Cycles*, *21*, GB4006, doi:10.1029/2006GB002907.

Emery, K. O. (1968), Relict sediments on continental shelves of world, *AAPG Bull.*, *52*(3), 445–464.

Fennel, K., et al. (2009), Modeling denitrification in aquatic sediments, *Biogeochemistry*, *93*, 159–178, doi:10.1007/s10533-008-9270-z.

Flögel, S., et al. (2011), Simulating the biogeochemical effects of volcanic CO_2 degassing on the oxygen–state of the deep ocean during the cenomanian/turonian anoxic event (OAE2), *Earth Planet. Sci. Lett.*, *305*(3–4), 371–384.

Galloway, J. N., et al. (2004), Nitrogen cycles: Past, present, and future, *Biogeochemistry*, *70*(2), 153–226, doi:10.1007/s10533-004-0370-0.

Garcia, H. E., R. A. Locarnini, T. P. Boyer, and J. I. Antonov (2006a), *World Ocean Atlas 2005*, vol. 3, *Dissolved Oxygen, Apparent Oxygen Utilization, and Oxygen Saturation*, *NOAA Atlas NESDIS*, vol. 63, edited by S. Levitus, 342 pp., NOAA, Silver Spring, Md.

Garcia, H. E., R. A. Locarnini, T. P. Boyer, and J. I. Antonov (2006b), *World Ocean Atlas 2005*, vol. 4, *Nutrients (Phosphate, Nitrate, Silicate)*, *NOAA Atlas NESDIS*, vol. 64, edited by S. Levitus, 396 pp., NOAA, Silver Spring, Md.

Glud, R. N. (2008), Oxygen dynamics of marine sediments, *Mar. Biol. Res.*, *4*(4), 243–289.

Gruber, N. (2004), The dynamics of the marine nitrogen cycle and its influence on the atmospheric CO_2 variations, in *The Ocean Carbon Cycle and Climate*, *NATO ASI Ser.*, vol. 40, edited by M. Follows and T. Oguz, pp. 97–148, Kluwer Acad., Dordrecht, Netherlands.

Gruber, N., and J. L. Sarmiento (1997), Global patterns of marine nitrogen fixation and denitrification, *Global Biogeochem. Cycles*, *11*(2), 235–266, doi:10.1029/97GB00077.

Hammond, D. E., et al. (1999), Diagenesis of carbon and nutrients and benthic exchange in sediments of the northern Adriatic Sea, *Mar. Chem.*, *66*(1–2), 53–79, doi:10.1016/S0304-4203(99)00024-9.

Hartnett, H. E., and A. H. Devol (2003), Role of a strong oxygen-deficient zone in the preservation and degradation of organic matter: A carbon budget for the continental margins of northwest Mexico and Washington State, *Geochim. Cosmochim. Acta*, *67*, 247–264.

Helly, J. J., and L. A. Levin (2004), Global distribution of naturally occurring marine hypoxia on continental margins, *Deep Sea Res., Part I*, *51*, 1159–1168, doi:10.1016/j.dsr.2004.03.009.

Hensen, C., H. Landenberger, M. Zabel, and H. D. Schulz (1998), Quantification of diffusive benthic fluxes of nitrate, phosphate and silicate in the southern Atlantic Ocean, *Global Biogeochem. Cycles*, *12*(1), 193–210, doi:10.1029/97GB02731.

Huettel, M., and A. Rusch (2000), Transport and degradation of phytoplankton in permeable sediment, *Limnol. Oceanogr.*, *45*(3), 534–549.

Ingall, E., and R. Jahnke (1994), Evidence for enhanced phosphorus regeneration from marine sediments overlain by oxygen depleted waters, *Geochim. Cosmochim. Acta*, *58*(11), 2571–2575.

Jahnke, R. (1996), The global ocean flux of particulate organic carbon: Areal distribution and magnitude, *Global Biogeochem. Cycles*, *10*, 71–88, doi:10.1029/95GB03525.

Jahnke, R., et al. (2005), Organic matter remineralization and porewater exchange rates in permeable South Atlantic Bight continental shelf sediments, *Cont. Shelf Res.*, *25*(12–13), 1433–1452, doi:10.1016/j.csr.2005.04.002.

Koné, V., E. Machu, P. Penven, V. Andersen, V. Garçon, P. Fréon and H. Demarcq (2005), Modeling the primary and secondary productions of the southern Benguela upwelling system: A comparative study through two biogeochemical models, *Global Biogeochem. Cycles*, *19*, GB4021, doi:10.1029/2004GB002427.

Lachkar, Z., and N. Gruber (2011), What controls biological production in coastal upwelling systems? Insights from a comparative modeling study, *Biogeosciences*, *8*, 2961–2976, doi:10.5194/bg-8-2961-2011.

Locarnini, R. A., A. V. Mishonov, J. I. Antonov, T. P. Boyer, and H. E. Garcia (2006), *World Ocean Atlas 2005*, vol. 1, *Temperature*, *NOAA Atlas NESDIS*, vol. 61, edited by S. Levitus, 182 pp., NOAA, Silver Spring, Md.

Martin, J. H., et al. (1987), Vertex: Carbon cycling in the northeast pacific, *Deep Sea Res., Part A*, *34*(2), 267–285, doi:10.1016/0198-0149(87)90086-0.

Meeson, B. W., F. E. Coprew, J. M. P. McManus, D. M. Myers, J. W. Closs, K.-J. Sun, D. J. Sunday, and P. J. Sellers (1995), *ISLSCP Initiative I—Global Data Sets for Land-Atmosphere Models, 1987–1988* [CD–ROM], NASA, Greenbelt, Md.

Middelburg, J. J., K. Soetaert, P. M. J. Herman, and C. H. R. Heip (1996), Denitrification in marine sediments: A model study, *Global Biogeochem. Cycles*, *10*(4), 661–673, doi:10.1029/96GB02562.

Middelburg, J. J., et al. (1997), Empirical relationships for use in global diagenetic models, *Deep Sea Res., Part I*, *44*(2), 327–344, doi:10.1016/S0967-0637(96)00101-X.

Müller, P. J. (1977), C/N ratios in Pacific deep-sea sediments: Effect of inorganic ammonium and organic nitrogen compounds sorbed by clays, *Geochim. Cosmochim. Acta*, *41*, 765–776, doi:10.1016/0016-7037(77)90047-3.

Muller-Karger, F. E., R. Varela, R. Thunell, R. Luerssen, C. M. Hu, and J. J. Walsh (2005), The importance of continental margins in the global carbon cycle, *Geophys. Res. Lett.*, *32*, L01602, doi:10.1029/2004GL021346.

Otte, S., J. G. Kuenen, L. P. Nielsen, H. W. Paerl, J. Zopfi, H. N. Schulz, A. Teske, B. Strotmann, V. A. Gallardo, and B. B. Jøørgensen (1999), Nitrogen, carbon, and sulfur metabolism in natural Thioploca samples, *Appl. Environ. Microbiol.*, *65*, 3148–3157.

Rao, A. M. F., et al. (2007), Respiration and denitrification in permeable continental shelf deposits on the south Atlantic Bight: Rates of carbon and nitrogen cycling from sediment column experiments, *Cont. Shelf Res.*, *27*(13), 1801–1819, doi:10.1016/j.csr.2007.03.001.

Redfield, A. C., et al. (1963), The influence of organisms on the composition of seawater, in *The Sea*, vol. 2, *The Composition of Sea Water: Comparative and Descriptive Oceanography*, edited by M. N. Hill, pp. 26–77, Wiley Interscience, Hoboken, N. J.

Roden, G. I. (1958), Oceanographic and meteorological aspects of the Gulf of California, *Pac. Sci.*, *12*(1), 21–45.

Romaniello, S. J., and L. A. Derry (2010), An intermediate-complexity model for simulating marine biogeochemistry in deep time: Validation against the modern global ocean, *Geochem. Geophys. Geosyst.*, *11*, Q08001, doi:10.1029/2009GC002711.

Rullkötter, J. (2006), Organic matter: The driving force for early diagenesis, in *Marine Geochemistry*, 2nd ed., edited by H. D. Schulz and M. Zabel, pp. 125–168, Springer, Berlin, doi:10.1007/3-540-32144-6_4.

Rysgaard, S., et al. (1994), Oxygen regulation of nitrification and denitrification in sediments, *Limnol. Oceanogr.*, *39*(7), 1643–1652, doi:10.4319/lo.1994.39.7.1643.

Sarmiento, J. L., and N. Gruber (2006), Organic matter production, in *Ocean Biogeochemical Dynamics*, pp. 102–172, Princeton Univ. Press, Princeton, N.J.

Schwartz, M. C., et al. (2009), Sedimentary denitrification rates across the Arabian Sea oxygen minimum zone, *Deep Sea Res., Part II*, *56*, 324–332, doi:10.1016/j.dsr2.2008.05.028.

Seitzinger, S., J. A. Harrison, J. K. Bohlke, A. F. Bouwman, R. Lowrance, B. Peterson, C. Tobias, and G. Van Drecht (2006), Denitrification across landscapes and waterscapes: A synthesis, *Ecol. Appl.*, *16*, 2064–2090, doi:10.1890/1051-0761(2006)016[2064:DALAWA]2.0.CO;2.

Sloss, P. W. (1988), Data Announcement 88-MGG-02, Digital Relief of the Surface of the Earth, ETOPO5 5-Minute Gridded Elevation Data, http://www.ngdc.noaa.gov/mgg/global/etopo5.HTML, Natl. Geophys. Data Cent., Boulder, Colo.

Soetaert, K., J. J. Middelburg, P. M. J. Herman, and K. Buis (2000), On the coupling of benthic and pelagic biogeochemical models, *Earth Sci. Rev.*, *51*, 173–201, doi:10.1016/S0012-8252(00)00004-0.

Somes, C. J., A. Schmittner, E. D. Galbraith, M. F. Lehmann, M. A. Altabet, J. P. Montoya, R. M. Letelier, A. C. Mix, A. Bourbonnais, and M. Eby (2010), Simulating the global distribution of nitrogen isotopes in the ocean, *Global Biogeochem. Cycles*, *24*, GB4019, doi:10.1029/2009GB003767.

Thamdrup, B., and T. Dalsgaard (2002), Production of N_2 through anaerobic ammonium oxidation coupled to nitrate reduction in marine sediments, *Appl. Environ. Microbiol.*, *68*, 1312–1318, doi:10.1128/AEM.68.3.1312-1318.2002.

Thunell, R. C. (1998), Seasonal and annual variability in particle fluxes in the Gulf of California: A response to climate forcing, *Deep-Sea Res., Part I*, *45*, 2059–2083, doi:10.1016/S0967-0637(98)00053-3.

Thullner, M., A. W. Dale, and P. Regnier (2009), Global-scale quantification of mineralization pathways in marine sediments: A reaction-transport modeling approach, *Geochem. Geophys. Geosyst.*, *10*, Q10012, doi:10.1029/2009GC002484.

Tiedje, J. M. (1988), Ecology of denitrification and dissimilatory nitrate reduction to ammonium, in *Biology of Anaerobic Microorganisms*, edited by A. J. B. Zehnder, pp. 179–244, Wiley, New York.

Vance-Harris, C., and E. Ingall (2005), Denitrification pathways and rates in the sandy sediments of the Georgia continental shelf, USA, *Geochem. Trans.*, *6*(1), 12–18.

Van Mooy, B. A. S., R. G. Keil, and A. H. Devol (2002), Impact of suboxia on sinking particulate organic carbon: Enhanced carbon flux and preferential degradation of amino acids via denitrification, *Geochim. Cosmochim Acta.*, *66*(3), 457–465.

Wallmann, K. (2010), Phosphorus imbalance in the global ocean?, *Global Biogeochem. Cycles*, *24*, GB4030, doi:10.1029/2009GB003643.